Three-dimensional noncontact manipulation by opposite ultrasonic phased arrays

2014 Jpn. J. Appl. Phys. 53 07KE07

(http://iopscience.iop.org/1347-4065/53/7S/07KE07)

Japanese Journal of Applied Physics **53**, 07KE07 (2014) **REGULAR PAPER**
http://dx.doi.org/10.7567/JJAP.53.07KE07

Three-dimensional noncontact manipulation by opposite ultrasonic phased arrays

Takayuki Hoshi[1]*, Yoichi Ochiai[2], and Jun Rekimoto[2,3]

[1]*The Center for Fostering Young and Innovative Researchers, Nagoya Institute of Technology, Nagoya 466-8555, Japan*
[2]*The University of Tokyo, Bunkyo, Tokyo 113-0033, Japan*
[3]*Sony SCL, Shinagawa, Tokyo 141-0022, Japan*
E-mail: star@nitech.ac.jp

Received November 25, 2013; revised February 18, 2014; accepted April 14, 2014; published online June 12, 2014

A three-dimensional acoustic manipulation in air is presented. Two arrays of ultrasonic transducers are arranged opposite each other, generating a localized standing wave at an arbitrary position through the phased-array focusing technique. Small particles are suspended in the nodes of the standing wave and also manipulated according to the position of the standing wave. This paper gives the following principles of the proposed method: the theory of acoustic levitation, the ultrasonic phased array, and the estimation of the radial and axial forces. It was experimentally confirmed that particles of 0.6 mm diameter are trapped in the nodes. The length of the localized standing wave, the suspension endurance, and the size of the work space were investigated. It was also demonstrated that a mass of particles can be scooped up when the localized standing wave moves through the mass.

1. Introduction

Conventional studies on acoustic levitation in air are divided into two types (Table I). One is near-field acoustic levitation (NFAL) in which near-field effects are utilized to levitate objects within a short range (less than 1 mm). Hashimoto et al. demonstrated that a planar object is levitated above a plate vibrated by a bolted Langevin transducer (BLT)[1)] and later developed a linear slider based on NFAL.[2)] Hoshina et al.[3)] expanded NFAL to 2D manipulation with an array of their original annular transducers.

The other is standing-wave acoustic levitation (SWAL) in which a standing wave is utilized to suspend objects at a relatively longer range (up to 150 mm) and many studies have been reported. Whymark[4)] firstly demonstrated that small particles and droplets are trapped in the nodes of the standing wave in air. Recently, Xie et al.[5)] have demonstrated that small animals can be levitated. Their setup consisted of a pair of a BLT and a reflector. Kozuka et al.[6)] and Weber et al.[7)] levitated and further manipulated particles of expanded polystyrene and droplets of various types of liquid, respectively. Two BLTs are arranged face-to-face and generate a standing wave of ultrasound beam between them. Particles and droplets were transported along the acoustic axis by controlling the phase difference between the transducers. Ito et al.[8)] utilized the horizontal traveling wave between vibrator and reflector plates to transport particles along them. Foresti et al.[9)] transported multiple droplets horizontally to mix them by using an array of BLTs and a reflector. They also levitated, rotated, and transported a stick much longer than the wavelength of ultrasound.

Kono et al.[10,11)] developed a system that makes particles wonder over a floor by using an airborne ultrasound focusing device[12,13)] (AUFD) instead of a BLT. The AUFD generates an ultrasonic focal point at an arbitrary position based on the phased-array focusing technique.[13,14)] It delivers ultrasound effectively farther than those observed in previous research studies (more than 150 mm). When the AUFD radiates ultrasound against a floor, a localized standing wave is generated near the floor by reflection and traps small particles at a fixed height. The particles are moved according to the position of the localized standing wave.

Table I. Studies on acoustic levitation. "Distance" is the distance from a transducer to an object for NFAL and to a reflector/another transducer for SWAL. "DOF" is the degree of freedom of transportation.

Method	Ref.	Distance (mm)	DOF	Objects (Size in mm)
NFAL	1	≤ 0.5	0	($65 \times 90 \times 1.1$)
	2	—	1	($75 \times 70 \times 2$)
	3	—	2	(21×21)
SWAL	4	150	0	Particles (—)
	4	—	0	Droplets (4)
	5	30	0	Animals (≤ 10)
	6	26	1	Particles (2–3)
	7	150	1	Droplets (≤ 3.5)
	8	13.5	1	Particles (2)
	9	7	2	Droplets (≤ 2)
	9	14	2	Stick (80 in length)
	10, 11	200	2	Particles (2)
	This study	520	3	Particles (0.6)

In this study, we demonstrate 3D manipulation based on SWAL by employing two AUFDs. The AUFDs are arranged opposite each other and generate ultrasonic focal points at the same position. The superposed focal point forms a beam of ultrasonic standing wave with a finite length, i.e., a focal depth. Then, a localized standing wave is formed at the focal point and traps small particles (Fig. 1) in air. This configuration provides the following features.

(1) The particles can be manipulated in all directions according to the movement of the localized standing wave based on the phase-delay control.
(2) The work space is much larger than those in previous research studies because the ultrasound wave is focused and hence delivered farther.
(3) The particles are kept trapped even when the acoustic axis is horizontal because the AUFDs provide a sufficient amplitude of ultrasound.

The following paper outlines, first, the principles of SWAL in our setup. Second, experiments and results are presented in Sect. 3. After some issues are discussed in Sect. 4, finally, Sect. 5 concludes this paper.

Fig. 1. (Color online) Levitation by opposed ultrasound phased arrays.

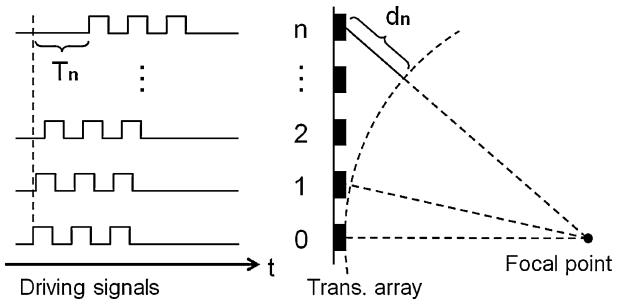

Fig. 2. Phased-array focusing technique.

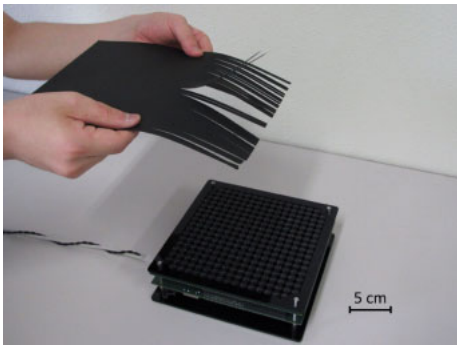

Fig. 3. (Color online) Previous usage of AUFD.[12] Paper strips held by hands are flipped up by the focused ultrasound.

2. Principles

2.1 Energy potential of ultrasonic standing wave

The acoustic levitation is based on the radiation pressure. It was mathematically explained by Gor'kov[15] and Nyborg,[16] and further discussed by, e.g., Barmatz and Collas,[17] Takeuchi,[18] and Kozuka et al.[19] The force $\boldsymbol{F}$ (N) acting on a small sphere is written as

$$\boldsymbol{F} = -V\nabla U, \tag{1}$$

$$U = -B\langle K_a\rangle + (1-\gamma)\langle P_a\rangle. \tag{2}$$

Here, V (m^3) is the volume of the small particle and U (J/m^3) is the potential energy per unit volume of an ultrasonic standing wave. K_a (J/m^3) and P_a (J/m^3) are the kinetic and potential energy densities of ultrasound, respectively. $\langle\cdot\rangle$ means the time average. B and γ are defined as

$$B \equiv \frac{3(\rho-\rho_0)}{2\rho+\rho_0}, \tag{3}$$

$$\gamma \equiv \frac{\beta}{\beta_0}. \tag{4}$$

Here, ρ (kg/m^3) and ρ_0 (kg/m^3) are the weight densities of the sphere and medium, respectively. β (N/m^2) and β_0 (N/m^2) are the compression ratios of the sphere and medium, respectively.

We assume an ultrasonic standing wave along the z-axis. Its sound pressure p (Pa) is written as

$$p = \sqrt{2}A\, g(x,y)\cos\left(\frac{2\pi z}{\lambda}\right)e^{-\mathrm{j}\omega t}, \tag{5}$$

where A (Pa) is the RMS amplitude, $g(x,y)$ is the normalized cross-sectional distribution of the ultrasonic beam, λ (m) is the wavelength, and ω (rad/s) is the angular velocity. Then, $\langle K_a\rangle$ and $\langle P_a\rangle$ are written as

$$\langle K_a\rangle = g(x,y)\frac{A^2}{\rho_0 c^2}\sin^2\left(\frac{2\pi z}{\lambda}\right), \tag{6}$$

$$\langle P_a\rangle = g(x,y)\frac{A^2}{\rho_0 c^2}\cos^2\left(\frac{2\pi z}{\lambda}\right), \tag{7}$$

where $c = 340$ m/s is the speed of sound in the medium.

For simplicity, here we assume $\rho \gg \rho_0$ and $\beta \ll \beta_0$, which are true in most cases in air. Then, $B \approx 3/2$ and $\gamma \approx 0$. By substituting these [and also Eqs. (6) and (7)] into Eq. (2), U is approximated as

$$U \simeq g(x,y)^2\frac{A^2}{\rho_0 c^2}\left[-\frac{3}{2}+\frac{5}{2}\cos^2\left(\frac{2\pi z}{\lambda}\right)\right]. \tag{8}$$

2.2 Ultrasonic phased array

The AUFD was originally intended for irradiating a traveling wave of focused ultrasound and generating a noncontact force based on the acoustic radiation pressure (Fig. 3). In this study, two of the same devices are used to generate a standing wave and trap small particles in the nodes.

The AUFD generates a focal point of ultrasound in air based on the phased-array focusing technique.[13,14] This technique is well known and has been used, for example, to generate audible sound spots in air,[20] to trap microbubbles in fluid,[21] and to conduct high-intensity focused ultrasound (HIFU) treatment.[22–25] An array of ultrasonic transducers is used to generate a focal point at an arbitrary position. The time difference T_n (s) for the n-th transducer (Fig. 2) is determined as

$$T_n = \frac{d_n}{c}, \tag{9}$$

where d_n (m) is the difference between the distances from the focal point to the 0-th and n-th transducers.

Here, we express the spatial distribution of ultrasound by equations for further discussion below, although it can also be investigated by numerical calculation.[26–29] It is theoretically derived that the spatial distribution of ultrasound on the focal plane generated by a square transducer array is nearly sinc-function-shaped[13,14] and the normalized cross-sectional distribution $g(x,y)$ is written as

$$g(x,y) \simeq \mathrm{sinc}\left(\frac{2\pi x}{w}, \frac{2\pi y}{w}\right). \tag{10}$$

Here, the two-dimensional sinc function $\mathrm{sinc}(x,y)$ is defined as $\sin x \sin y/xy$. w (m) is the width of the main lobe parallel to the side of the square, which is defined as

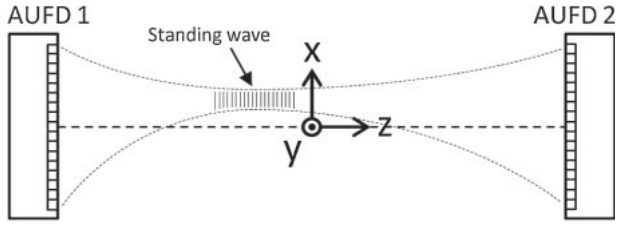

Fig. 4. Setup of noncontact manipulation system. A localized standing wave is generated at an arbitrary position.

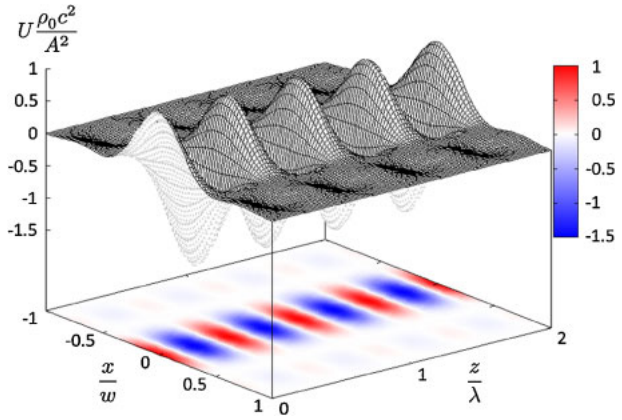

Fig. 5. (Color online) Potential energy distribution of a localized ultrasonic standing wave.

$$w \equiv \frac{2\lambda R}{D}, \tag{11}$$

where λ (m) is the wavelength, R (m) is the focal length, and D (m) is the side length of the square array.

The specifications of the latest version of the AUFD[12] are as follows. The amplitude of ultrasound is 162 dB SPL (2585 Pa RMS) at the center of the focal point with 285 transducers (Nippon Ceramic, T4010A1, 40 kHz, 10 mm in diameter) arranged within a $170 \times 170\,\mathrm{mm}^2$ square area. The size of the focal point w is, for example, 20 mm when the focal length R is set at 200 mm. The spatial resolution of the position of the focal point is 0.5 mm. The position can be updated at a rate of 1 kHz.

2.3 Radial and axial forces

A localized acoustic standing wave is formed when two AUFDs are arranged face-to-face (Fig. 4), generating focal points at the same position. Its cross section is written as Eq. (10) and it has a focal depth with a length of several centimeters. The distribution of the potential energy generated by the localized standing wave is shown in Fig. 5. Here, we derive the radial and axial forces from the potential energy and compare them. We assume that the distance between the two AUFDs is 400 mm and that the focal point is generated at the center (i.e., the origin of the coordinate in Fig. 4).

First, the radial force F_x (N) parallel to the x-axis through the center of a node is obtained as

$$F_x \equiv -V\frac{\partial U}{\partial x}\bigg|_{(y,z)=(0,\frac{\lambda}{4})}$$

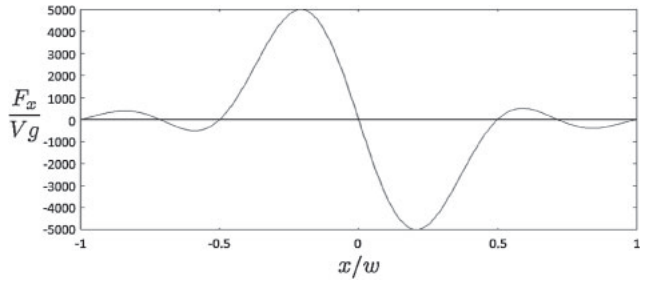

Fig. 6. Radial force per unit volume divided by the gravitational acceleration at $(y, z) = (0, \lambda/4)$.

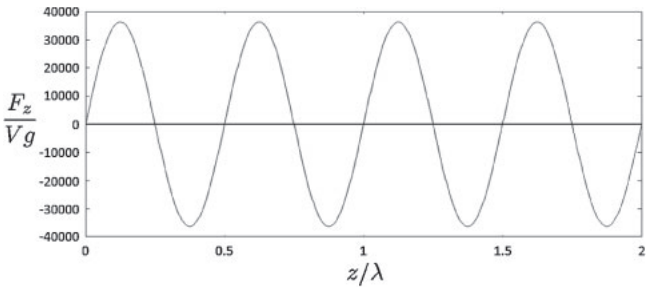

Fig. 7. Axial force per unit volume divided by the gravitational acceleration at $(x, y) = (0, 0)$.

$$\simeq \frac{A^2 V}{\rho_0 c^2}\frac{6\pi}{w}\left[\frac{\sin\left(\frac{2\pi x}{w}\right)\cos\left(\frac{2\pi x}{w}\right)}{\left(\frac{2\pi x}{w}\right)^2} - \frac{\sin^2\left(\frac{2\pi x}{w}\right)}{\left(\frac{2\pi x}{w}\right)^3}\right]. \tag{12}$$

The maximum value of F_x/Vg is $5.00 \times 10^3\,\mathrm{kg/m^3}$ at $x \approx -0.2w$ (Fig. 6), where $g = 9.8\,\mathrm{m/s^2}$ is the gravitational acceleration and $A = 5170$ Pa. This means that a material can be levitated by F_x if its weight density is lower than that value. For example, the weight density of polystyrene is around $1.0 \times 10^3\,\mathrm{kg/m^3}$. Note that not only the weight density but also the size and shape of objects are important factors for determining whether they can be trapped in the nodes.

Second, the axial force F_z (N) along the z-axis is obtained as

$$F_z \equiv -V\frac{\partial U}{\partial z}\bigg|_{(x,y)=(0,0)} \simeq \frac{A^2 V}{\rho_0 c^2}\frac{10\pi}{\lambda}\sin\left(\frac{2\pi z}{\lambda}\right)\cos\left(\frac{2\pi z}{\lambda}\right). \tag{13}$$

The maximum value of F_z/Vg is $3.63 \times 10^4\,\mathrm{kg/m^3}$ at, e.g., $z = \lambda/8$ (Fig. 7).

The maximum value of F_z is 7.3 times larger than that of F_x as derived above. This estimation agrees with the report that "the lateral restoring forces are about 10% of the levitation forces in the direction of the main sound beam" by Whymark[4] and gives the reason why F_z is mainly used in conventional studies rather than F_x. In this study, we can also utilize F_x to levitate objects because we have sufficient high-amplitude ultrasound owing to AUFDs.

3. Experiments and results

The system setup is shown in Fig. 4. Two AUFDs were

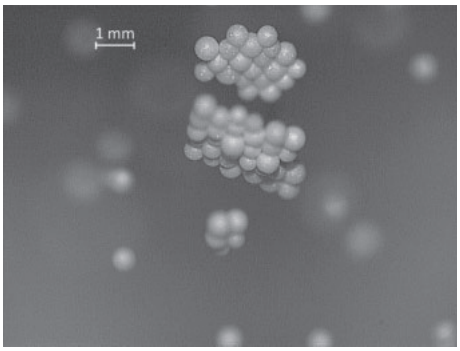

Fig. 8. Close-up photo of nodes taken with a 4000 fps high-speed camera. The particles are in a planar arrangement owing to the potential energy distribution.

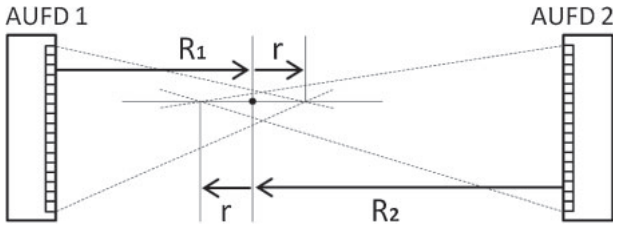

Fig. 9. Illustration of the offset r and the focal length R.

arranged face-to-face at a distance of 520 mm. This distance was tentatively determined. Note that the distance affects the size of the focal point and the intensity of the suspension force. The middle point between the AUFDs was taken as the original point of the coordinate. The z-axis was perpendicular to the radiation surfaces of the AUFDs. Expanded polystyrene particles (0.6 mm in average diameter) were used as levitated objects. The amplitude of ultrasound was set at 70% of the maximum. It was because the airflow accompanying the ultrasound beam or other factors prevented particles from entering the beam or from being suspended stably when the amplitude was large.

3.1 Particles in nodes

The particles trapped in the nodes of the ultrasonic standing wave were observed with a 4000 fps high-speed camera. Figure 8 shows that dozens of particles were appressed to each other and formed a single layer perpendicular to the acoustic axis. This indicates that the axial force is larger than the radial force and agrees with the discussion in Sect. 2.3.

3.2 Length of localized standing wave

Basically, a localized standing wave is generated when the AUFDs generate focal points at the same position. In addition, it was experimentally found that the offset r (m) of the focal length (Fig. 9) increases or decreases the length of the standing wave. The length of the localized standing wave was investigated by changing the offset r from -70 to 120 mm at 10 mm intervals. The center distance between the end particles was recorded after sprinkling particles over the localized standing wave at each offset value.

The results are shown in Fig. 10. The localized standing wave is longest (152 mm, i.e., 36 occupied nodes) when

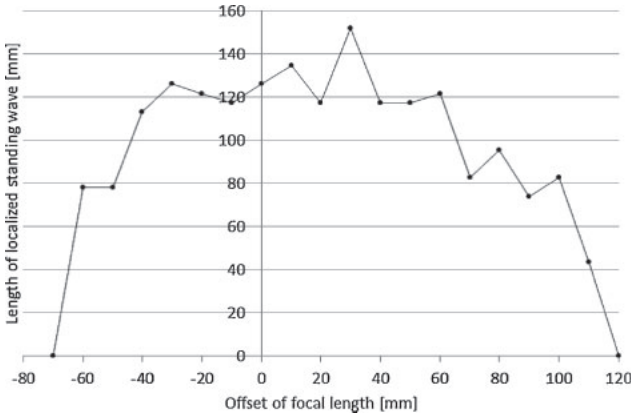

Fig. 10. Experimental results of the length of the localized standing wave vs the offset.

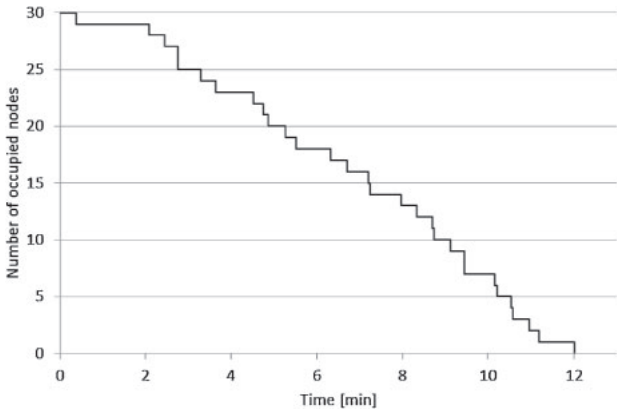

Fig. 11. Number of occupied nodes recorded over time.

$r = 30$ mm. This offset value is used in the following experiments.

3.3 Suspension endurance

The suspension endurance was studied to confirm the stability of the proposed method. The standing wave was fixed at the center and the particles were sprinkled over it. The number of nodes occupied by the particles was recorded over time.

The results are shown in Fig. 11. There were 30 nodes at first. Their number gradually decreased and became half after around 7 min. It was observed that all the nodes gradually moved together toward one of the AUFDs and they lost particles when they reached the end of the localized standing wave. This movement may be caused by the difference in frequency between the two ultrasonic beams.[6] This could be due to the different heat conditions of the AUFDs, which may affect the clock speed. Other effects were negligible and it is expected that the endurance will be longer if the conditions of the AUFDs are better adjusted.

3.4 Size of work space

The size of the work space was studied here. First, the localized standing wave was moved along the x-axis at a speed of 25 mm/s [Fig. 12(a)]. The particles at both ends were lost around $x = 50$ mm (2 s) and the particle at the

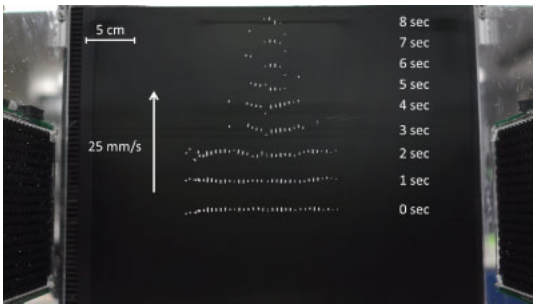

(a)

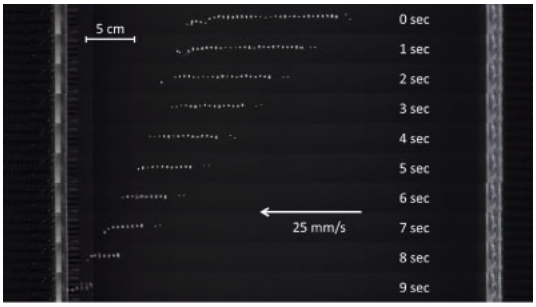

(b)

Fig. 12. (Color online) Time series of the movement of the localized standing wave. Multiple photos are superimposed in (a) and aligned in (b). (a) Along the x-axis. (b) Along the z-axis.

center was kept up to $x = 300$ mm (out of the observed area). Second, the localized standing wave was moved along the z-axis at a speed of 25 mm/s [Fig. 12(b)]. The particle at the center of the standing wave dropped around $z = -100$ mm (4 s). The movement along the y-axis is thought to be similar to that of the x-axis. For example, by limiting our focus to the 8 nodes at the center, they can be manipulated when $|x| \leq 125$ mm (5 s), $|y| \leq 125$ mm (5 s), and $|z| \leq 50$ mm (2 s).

3.5 Scooping up of particles

The particles were scooped up when the standing wave passed through a mass of particles. In this experiment, the mass was placed at $(x, y, z) = (-100, 0, 0)$ (mm). The standing wave started from $(x, y, z) = (-110, 0, 0)$ (mm) and moved up at a speed of 25 mm/s. Then, the nodes were successfully occupied by the particles (Fig. 13).

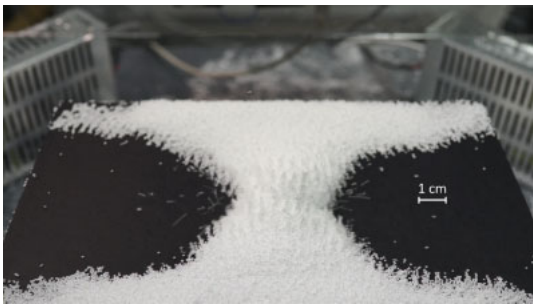

(a)

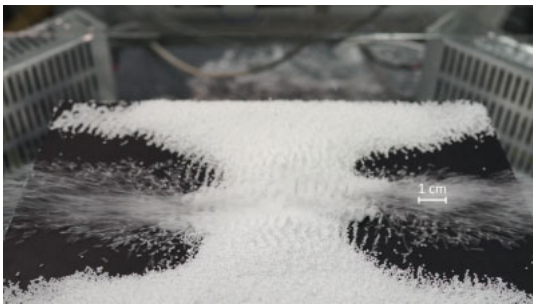

(b)

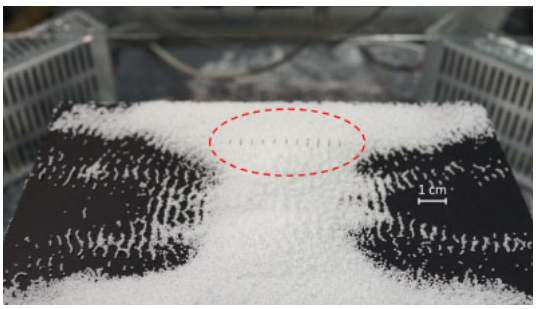

(c)

Fig. 13. (Color online) Scooping-up sequence: (a) 0.0, (b) 0.5, and (c) 1.0 s. The standing wave moves up through the mass of particles.

4. Discussion

There are multiple parameters to be adjusted for a specific application. For example, a higher value of the wavelength λ leads to a wider ultrasonic beam, a lower amplitude, and a longer interval between the nodes. A larger ratio of the focal length to the array size R/D also leads to a wider ultrasonic beam and a lower amplitude. These parameters should be determined considering limiting and required conditions.

Two AUFDs were arranged opposite each other in this study, but the number and arrangement of AUFDs are not limited. For example, multiple beams of ultrasonic standing waves generated by multiple pairs of AUFDs can be crossed and independently controlled. Furthermore, triangular and tetrahedral arrangements discussed for under-water conditions[30,31] can also be employed in air and then the nodes are limited within the intersection of the ultrasonic beams.

The AUFD generates not only a main lobe (a focal point) but also grating lobes at an angle of 40° because of the discrete transducer array.[13] It was observed that the intersections of the grating lobes also trapped small particles. It is better to take this phenomenon into account especially when the distance between the AUFDs is short.

5. Conclusions

We introduced a three-dimensional acoustic manipulation in this paper. A localized standing wave is generated at an arbitrary position by two opposite ultrasonic focusing devices. Expanded polystyrene particles (0.6 mm in diameter) are trapped in the nodes and also manipulated three-dimensionally according to the position of the standing wave. The principles of the proposed method were described and the forces parallel and perpendicular to the acoustic axis were derived, and the characteristics determined from the experimental results were reported. 36 nodes (152 mm in length) of the standing wave were occupied by particles at the maximum. They were kept suspended for several minutes in the current system. The work space for eight nodes was an area of $250 \times 250 \times 100\,\text{mm}^3$. A mass of particles was

scooped up by moving the localized standing wave through the mass.

Future works are roughly divided into three issues. The first issue is to improve and evaluate the performance of the developed acoustic manipulation system. Testing other objects such as larger/smaller particles, powder, liquid, fog, and so on is also included. The second issue is to explore applications. Examples of possible applications are (1) picking up, transporting, and placing small objects such as precision components, (2) fractionating objects of different densities, and (3) providing a physical interface floating in front of users. The last issue is to optimize the parameters such as the frequency of ultrasound, the distance between the AUFDs, and/or the focal length according to each application.

1) Y. Hashimoto, Y. Koike, and S. Ueha, J. Acoust. Soc. Am. **100**, 2057 (1996).
2) Y. Hashimoto, Y. Koike, and S. Ueha, J. Acoust. Soc. Am. **103**, 3230 (1998).
3) S. Hoshina, M. Aoyagi, H. Tamura, and T. Takano, Proc. USE, 2012, p. 81.
4) R. R. Whymark, Ultrasonics **13**, 251 (1975).
5) W. J. Xie, C. D. Cao, Y. J. Lü, Z. Y. Hong, and B. Wei, Appl. Phys. Lett. **89**, 214102 (2006).
6) T. Kozuka, K. Yasui, T. Tuziuti, A. Towata, and Y. Iida, Jpn. J. Appl. Phys. **46**, 4948 (2007).
7) R. J. K. Weber, C. J. Benmore, S. K. Tumber, A. N. Tailor, C. A. Rey, L. S. Taylor, and S. R. Byrn, Eur. Biophys. J. **41**, 397 (2012).
8) Y. Ito, D. Koyama, and K. Nakamura, Acoust. Sci. Technol. **31**, 420 (2010).
9) D. Foresti, M. Nabavi, M. Klingauf, A. Ferrari, and D. Poulikakos, Proc. Natl. Acad. Sci. U.S.A. **110**, 12549 (2013).
10) M. Kono, Y. Kakehi, and T. Hoshi, demonstrated at SIGGRAPH Asia 2013 Art Gallery, 2013.
11) M. Kono, T. Hoshi, and Y. Kakehi, Proc. Entertainment Computing, 2013, p. 41 [in Japanese].
12) T. Hoshi, Proc. Advances in Computer Entertainment Conf., 2012, p. 502.
13) T. Hoshi, submitted to Keisoku Jido Seigyo Gakkai Ronbunshi [in Japanese].
14) T. Hoshi, M. Takahashi, T. Iwamoto, and H. Shinoda, IEEE Trans. Haptics **3**, 155 (2010).
15) L. P. Gor'kov, Sov. Phys. Dokl. **6**, 773 (1962).
16) W. L. Nyborg, J. Acoust. Soc. Am. **42**, 947 (1967).
17) M. Barmatz and P. Collas, J. Acoust. Soc. Am. **77**, 928 (1985).
18) M. Takeuchi, Nippon Onkyo Gakkaishi **52**, 203 (1996) [in Japanese].
19) T. Kozuka, T. Tuziuti, H. Mitome, and T. Fukuda, Denshi Joho Tsushin Gakkai Ronbunshi A **J80-A**, 1654 (1997) [in Japanese].
20) K. Shinagawa, Y. Amemiya, H. Takemura, S. Kagami, and H. Mizoguchi, Proc. 2007 IEEE Int. Conf. Systems, Man and Cybernetics, 2007, p. 278.
21) N. Hosaka, R. Koda, S. Onogi, T. Mochizuki, and K. Masuda, Jpn. J. Appl. Phys. **52**, 07HF14 (2013).
22) Y. Ohara, Y. Shintaku, S. Horinouchi, M. Ikeuchi, and K. Yamanaka, Jpn. J. Appl. Phys. **51**, 07GB18 (2012).
23) S. Umemura, S. Yoshizawa, R. Takagi, Y. Inaba, and J. Yasuda, Jpn. J. Appl. Phys. **52**, 07HA02 (2013).
24) R. Narumi, K. Matsuki, S. Mitarai, T. Azuma, K. Okita, A. Sasaki, K. Yoshinaka, S. Takagi, and Y. Matsumoto, Jpn. J. Appl. Phys. **52**, 07HF01 (2013).
25) K. Nakamura, A. Asai, H. Sasaki, S. Yoshizawa, and S. Umemura, Jpn. J. Appl. Phys. **52**, 07HF10 (2013).
26) W. J. Xie and B. Wei, Phys. Rev. E **66**, 026605 (2002).
27) T. Kozuka, K. Yasui, T. Tuziuti, A. Towata, and Y. Iida, Jpn. J. Appl. Phys. **47**, 4336 (2008).
28) K. Otsu, S. Yoshizawa, and S. Umemura, Jpn. J. Appl. Phys. **50**, 07HC02 (2011).
29) N. Kawada, T. Yoda, N. Tagawa, T. Tsuchiya, and K. Okubo, Jpn. J. Appl. Phys. **51**, 07GG06 (2012).
30) T. Kozuka, T. Tuziuti, H. Mitome, F. Arai, and T. Fukuda, Proc. 2000 Int. Symp. Micromechatronics and Human Science, 2000, p. 201.
31) T. Kozuka, T. Tuziuti, H. Mitome, F. Arai, and T. Fukuda, Proc. 2001 JSME Annu. Meet., 2001, Vol. IV, p. 195 [in Japanese].